Argonne NATIONAL LABORATORY

... for a brighter future

U.S. Department of Energy

UChicago Argonne LLC

Office of Science U.S. DEPARTMENT OF ENERGY

A U.S. Department of Energy laboratory managed by UChicago Argonne, LLC

Use of high-energy X-ray microbeams for phase and strain mapping

Jon Almer and Ulrich Lienert

X-ray Science Division, ANL

Di-Jia Liu

Chemical Technology Division, ANL

Yana Qian

Northwestern University, Evanston, IL

APS Users Meeting

May 9, 2007

Outline

- Survey of probe sizes & techniques
- Sector 1-ID beamline for high-energy x-ray studies
- Solid oxide fuel cell
  - Phase and strain mapping with 1-d resolution
- Advanced gear steel
  - Strain mapping with 3-d resolution

Probe sizes of selected techniques

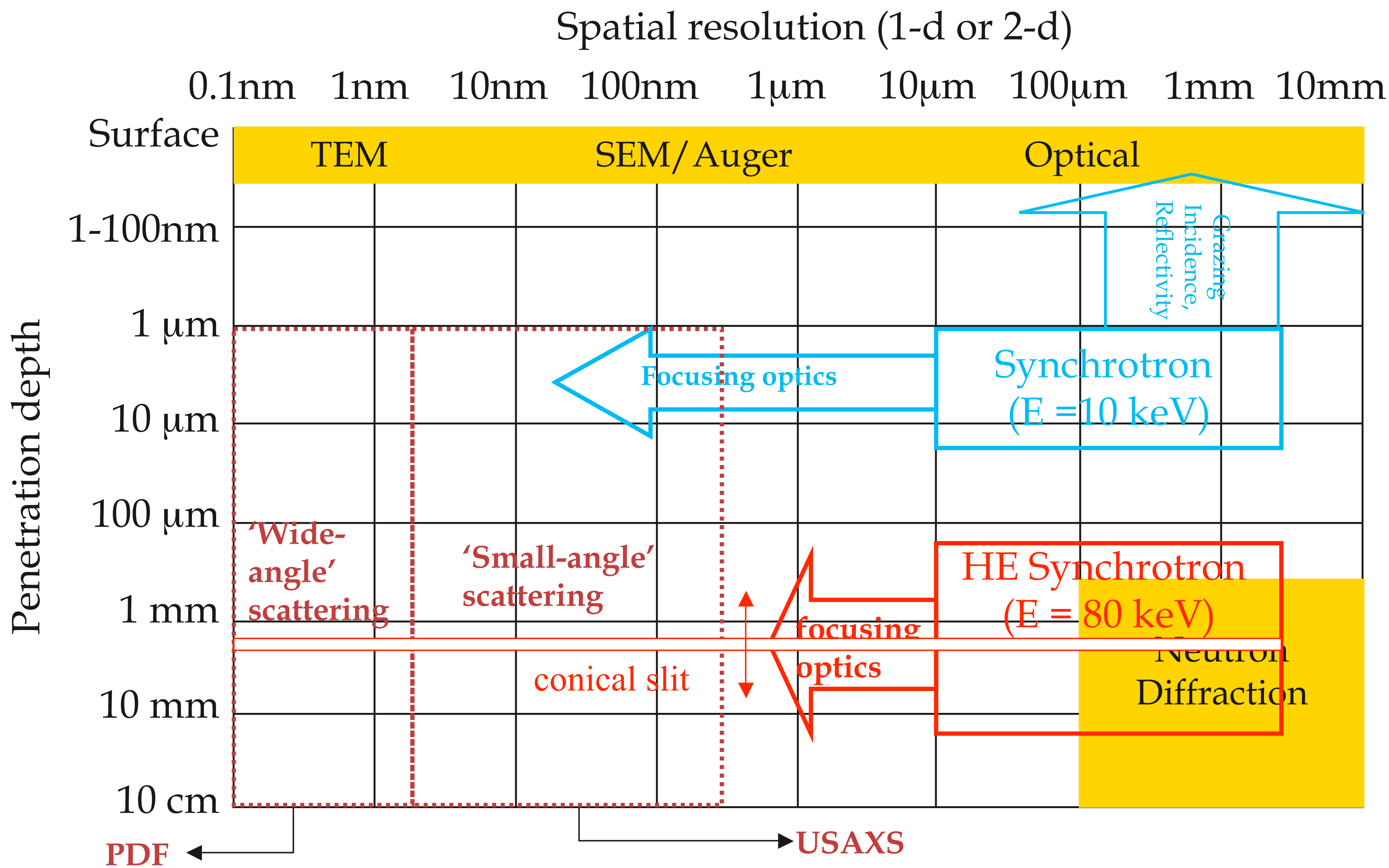

Strain scanning at the APS

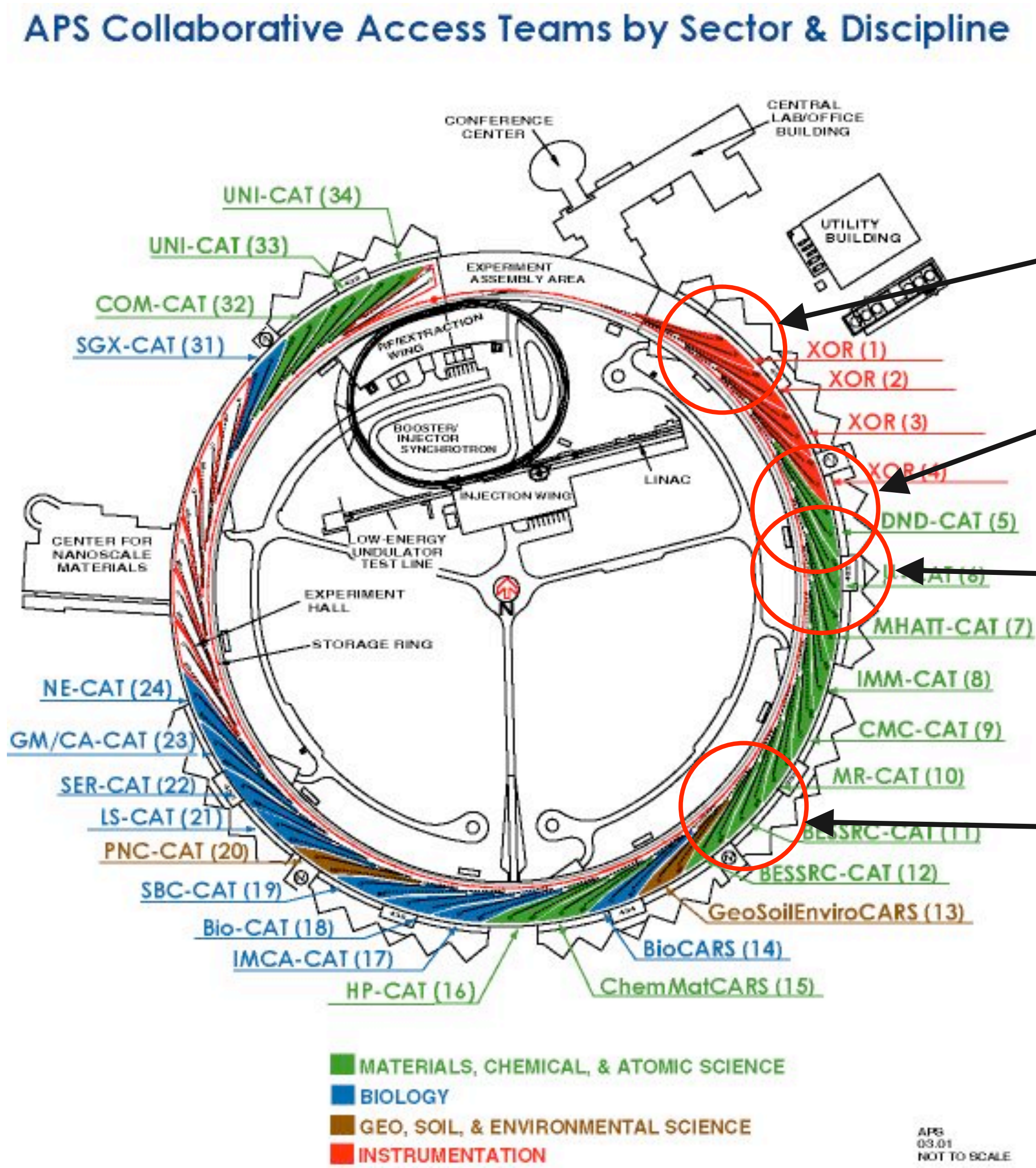

1-ID (XOR)
High-energy microfocusing

5-BM (DND)
Unoptomized bending magnet

6-ID (mu-CAT)
High-energy side station

11-ID (XOR)
Elliptical multipole wiggler
Triple axis diffractometer

APS 1-ID beamline

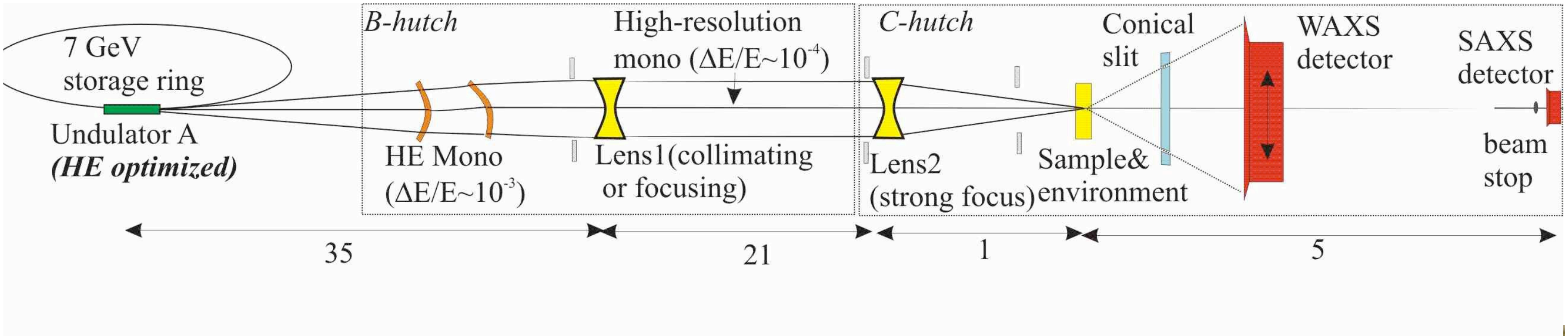

Key components
- Undulator
- Optimized HE optics (transverse resolution)
- Environment
    - Furnaces
    - Tensile/compressive loading rigs
    - MTS device
- Conical slit for longitudinal resolution
- Large (fast) area detectors

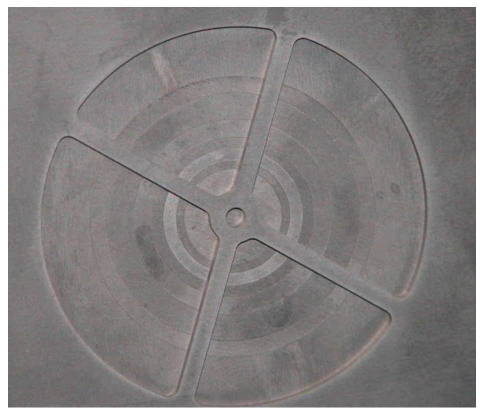

Conical slit (7 rings)

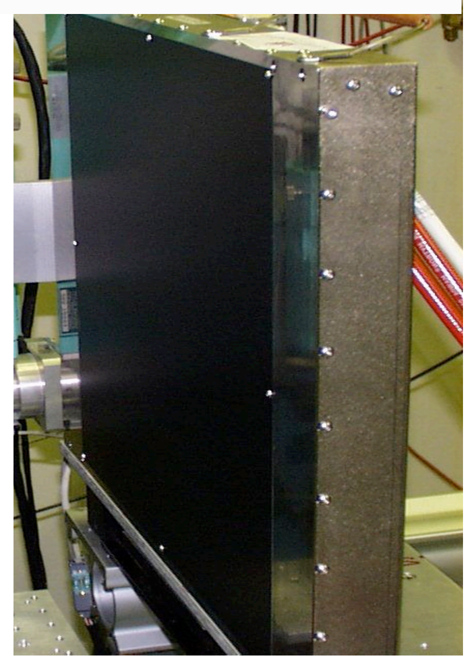

GE detector

Focusing using sawtooth refractive lenses

Collaborators: C. Ribbing (Uppsala) and B. Cederstrom (KTH), Sweden

Typical focal sizes:

18 um (weak focusing; zo:zi ~ 36:24 m)

1.5um (strong focusing; zo:zi ~ 60:1 m)

Even at 'strong focusing' the divergence is ~200 urad, low enough for high-quality diffraction

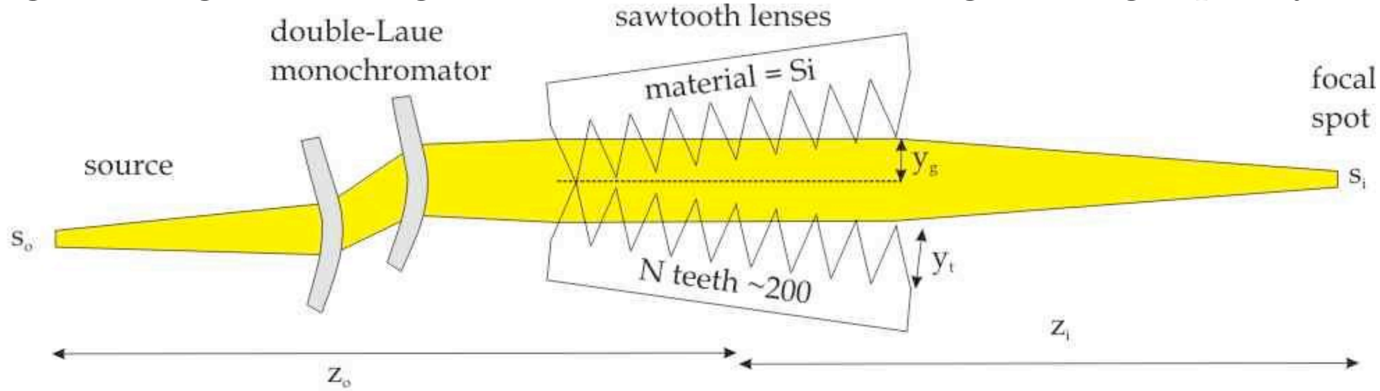

* high-energy monochromator is effectively brilliance preserving - minimal aberrations (some dependence on bend radii)

* use of pure material (single-crystal Si) gives minimal small-angle scattering from lens
* no absorption along lens optic axis (y=0)
* lens focus distance z_i can be varied through y_g
* theoretical image size:

$s_i=s_o(z_o/z_i)$

canted sawtooth projection y(z) is effectively parabolic (aberrations typically submicron)

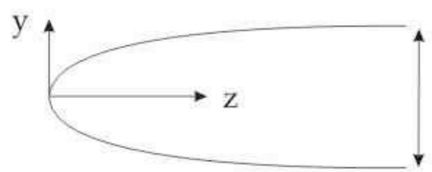

Physical aperture = $2*\min(y_g,y_t)$

Case study I: Phase and strain mapping in solid-oxide fuel cells

Collaborators:

Di-Jia Liu and Terry Cruze

Chemical Technology Division, ANL

Electrochemical Processes for Solid Oxide Fuel Cells (SOFCs)

Operating Principle of an SOFC

Anode

$H_2 + O^{2-} \rightarrow H_2O + 2e^-$

$CO + O^{2-} \rightarrow CO_2 + 2e^-$

H_2 & CO Oxidation Reactions

Cathode

$O_2 + 4e^- \rightarrow 2\ O^{2-}$

O_2 Reduction Reaction

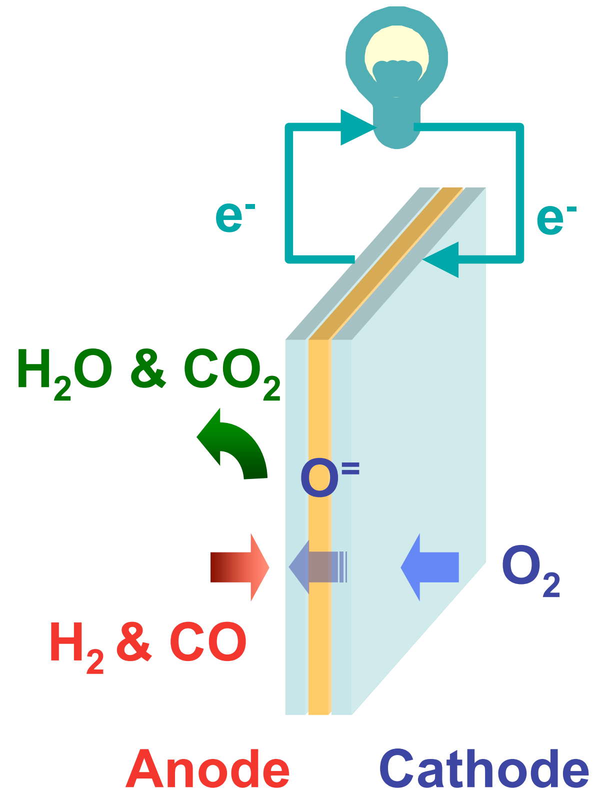

Artist's rendition of FutureGen power plant

Metallic Interconnect is Crucial in Reducing Material & Manufacturing Cost for SOFC

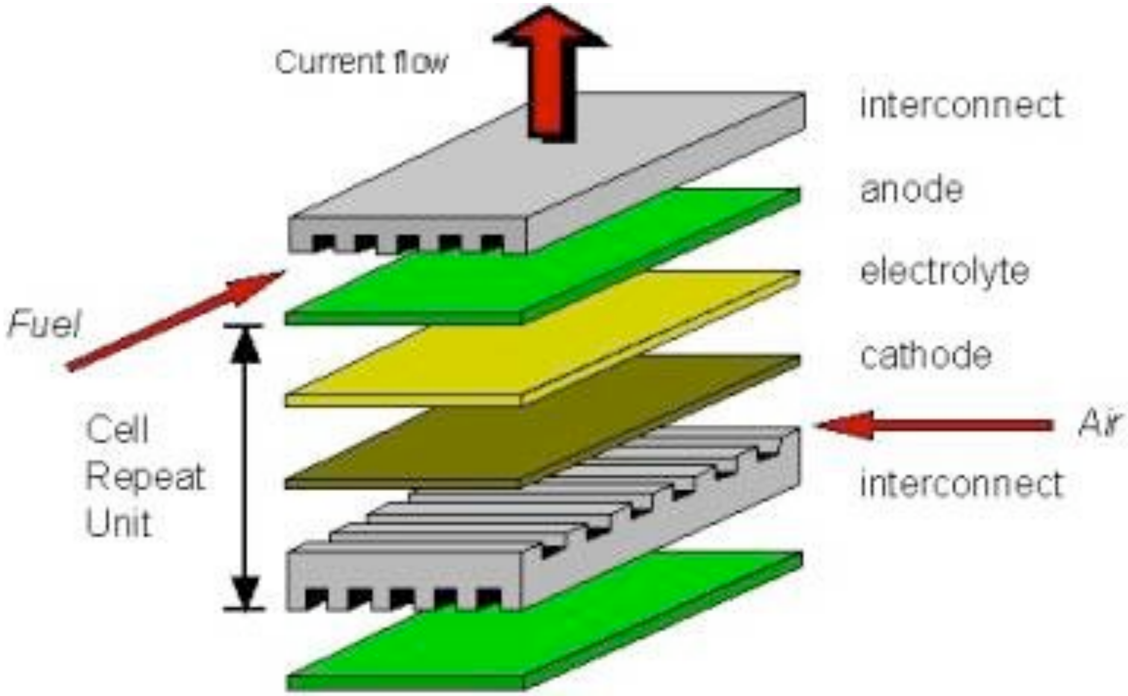

Cr Poisoning – A Material Challenge in SOFC Development

- SOFC deactivation is often associated with Cr accumulation in the cathode originated from metallic interconnect
- Knowledge of different Cr species & distribution is critical for understanding the deactivation mechanism
- Past experiments were limited to imaging (SEM, EDX, etc.) inconclusive in separating phase & distribution
- Conventional XRD method lacks spatial resolution and sensitivity

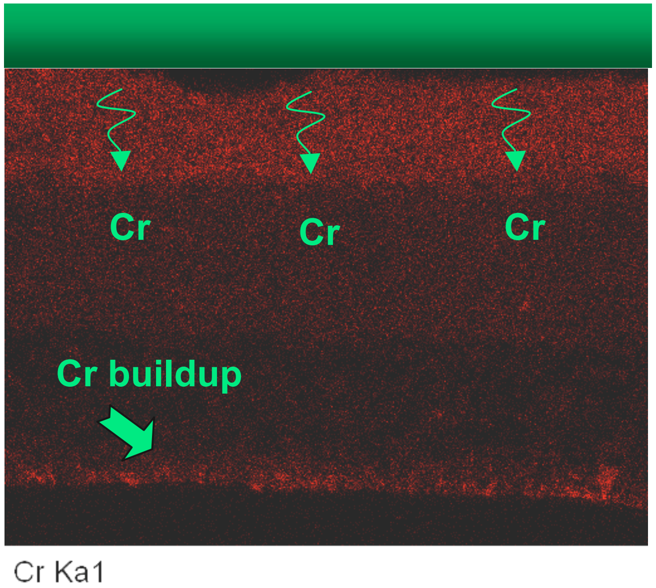

Significant enrichment of Cr is observed at the cathode and electrolyte interface

Use microfocused high-energy x-rays to map Cr phases, internal strains and phase stoichiometry

Button Cell Setup for Cr Poisoning Study

Test Conditions

- Current Density 250 mA/cm^2
- Air Flow 70 sccm
  - (at -1.15A, ~25% O_2 utilization)
- Fuel Flow 400 sccm (50% N_2, 50% H_2)
  - (at -1.15A, ~4% H_2 utilization)

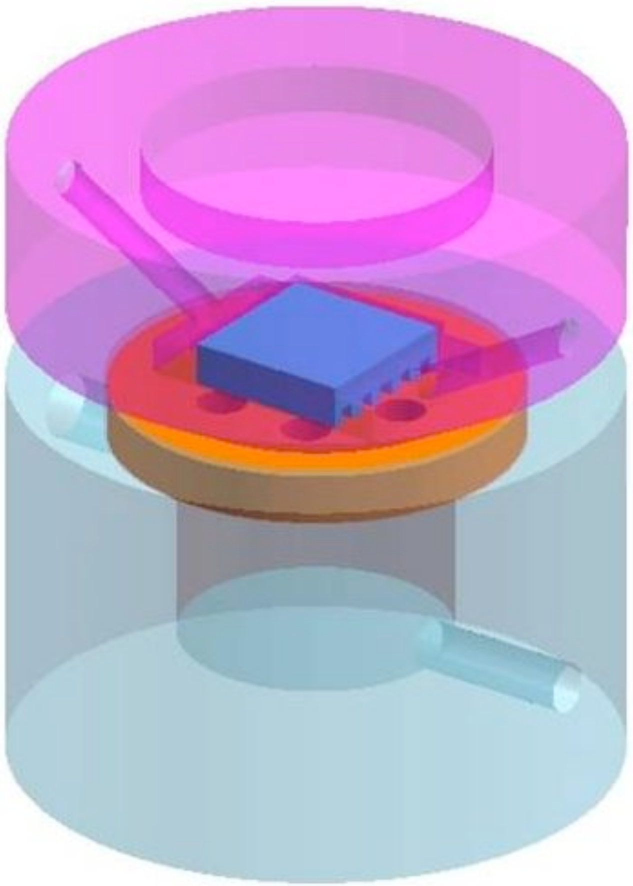

HEWAXS Characterization of Chromium Phase and Spatial Distributions in a Contaminated SOFC

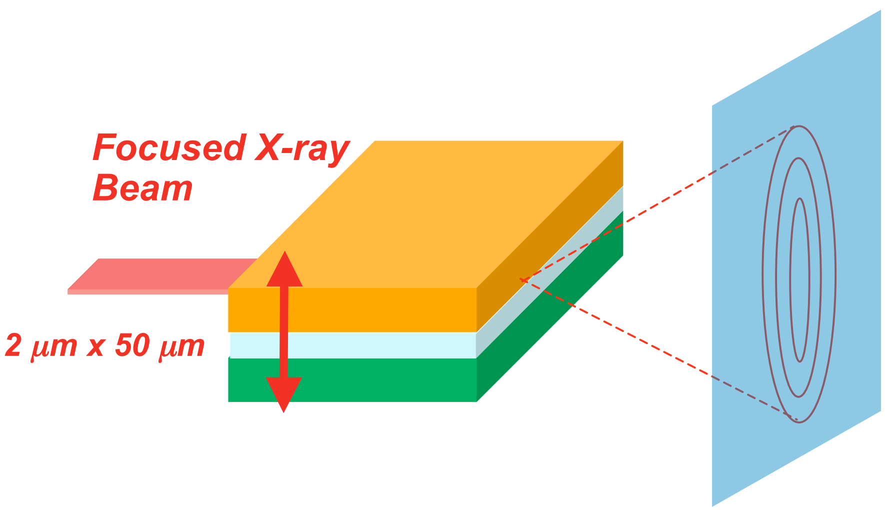

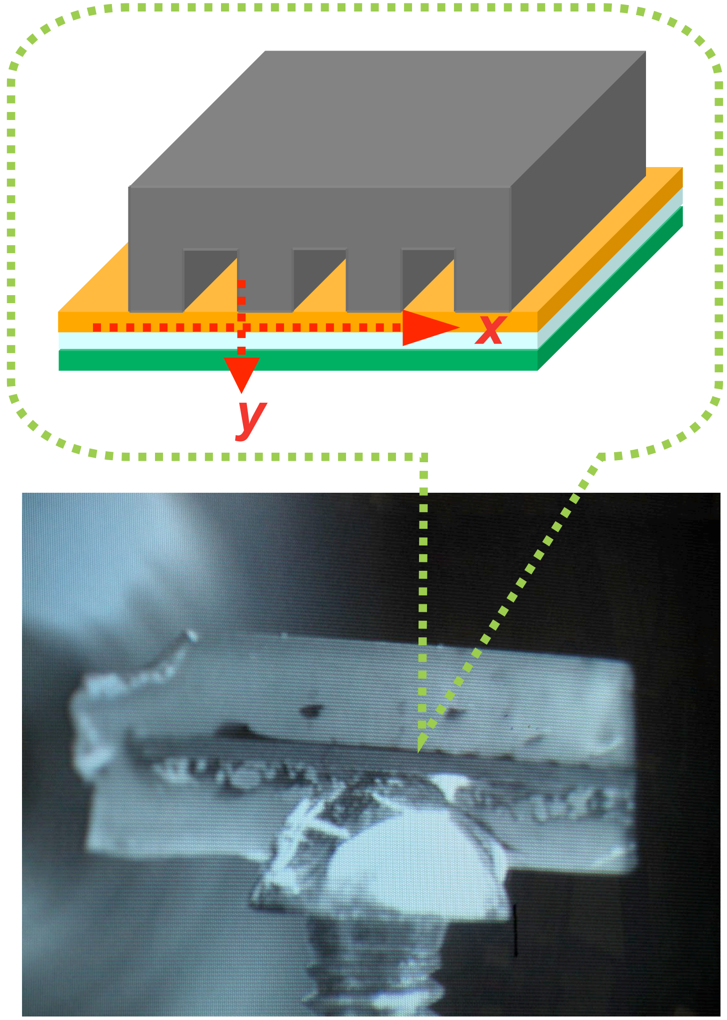

Cross-sectioned SOFC embedded in epoxy

Cross-section of SOFC Investigated (1mm thick)

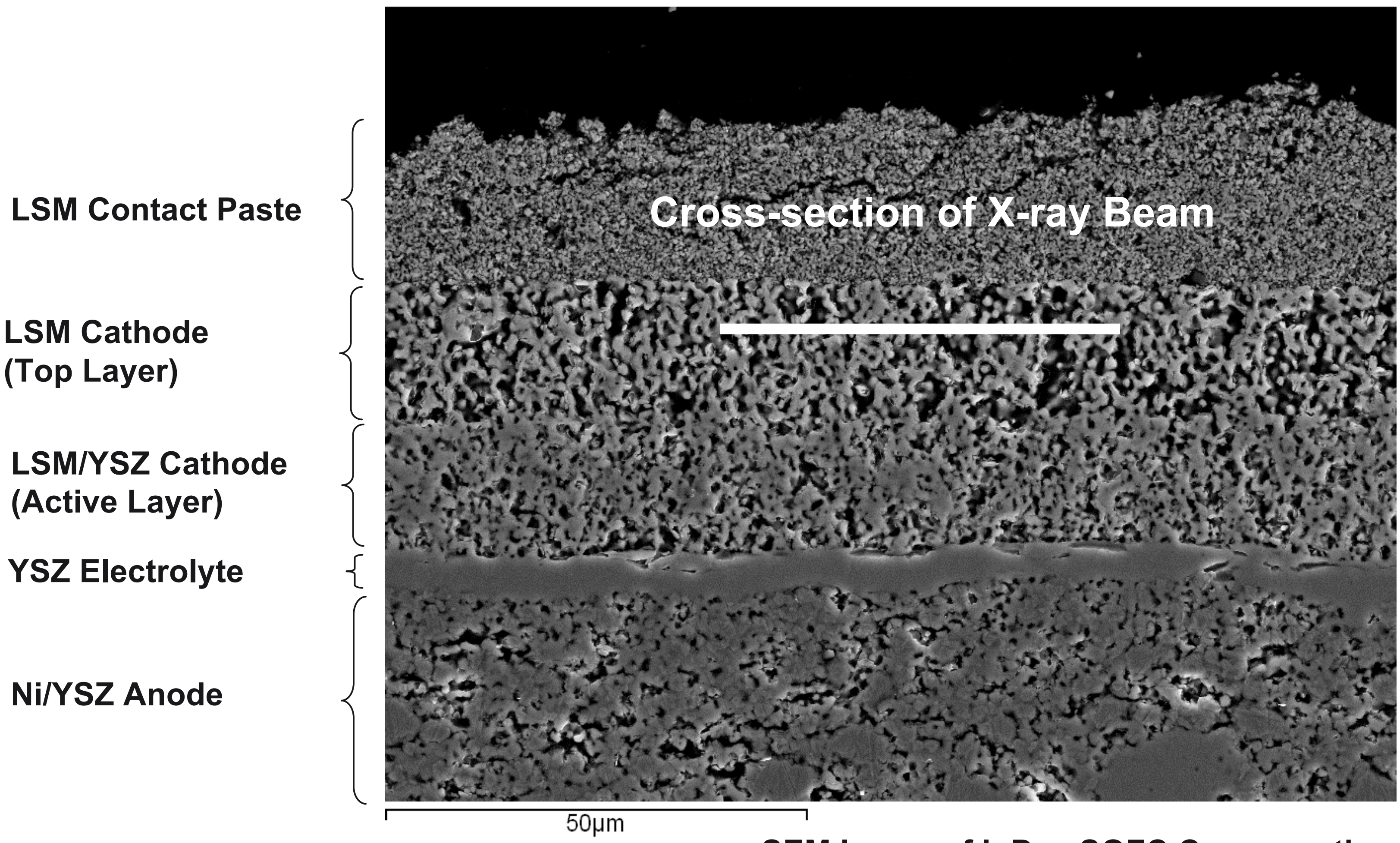

SEM Image of InDec SOFC Cross-section

Diffraction data from SOFC

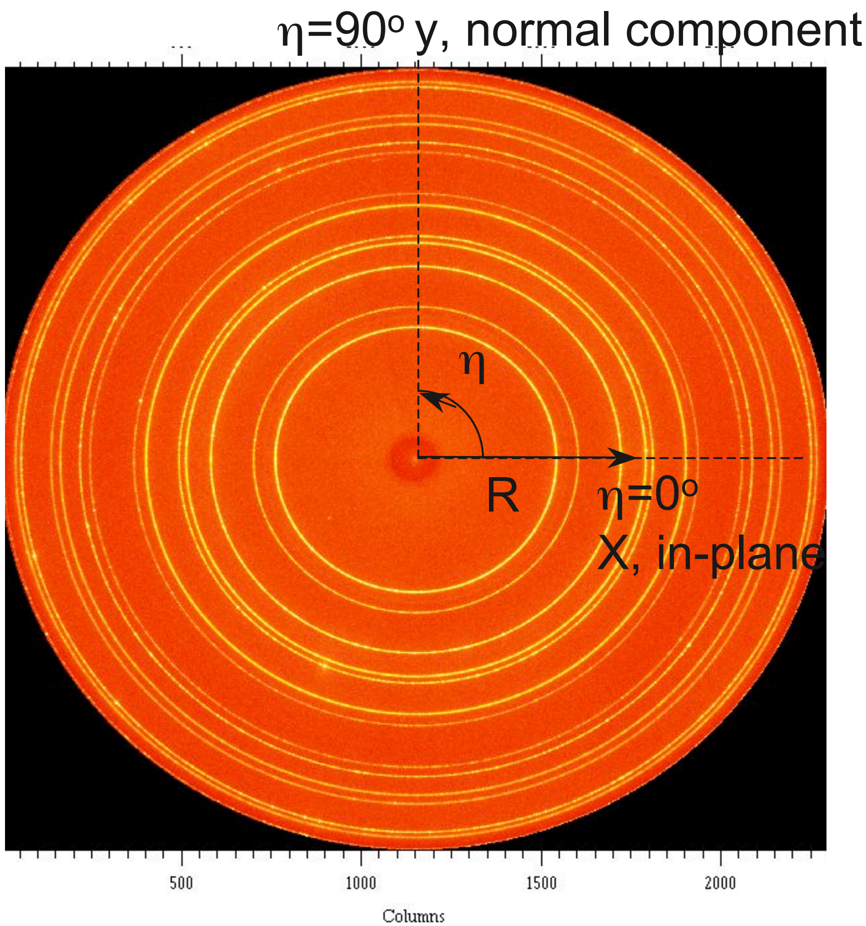

Typical pattern
Mar345, E=80.7 keV

Intensity

- Smooth & constant vs azimuth (fine grained, no texture)
- Phase composition analysis

Radius versus azimuth

- deviatoric strain
- $\Delta\varepsilon = -(r_{xx} - r_{yy})/r_{mean}$

Mean radius

- Estimate intraphase composition changes
- $\Delta d_{hkl}/d_{hkl} = -(r_{hkl} - r_{mean})/r_{mean}$

Argonne NATIONAL LABORATORY

Chromia and Manganese Chromium Spinel are Unambiguously Identified

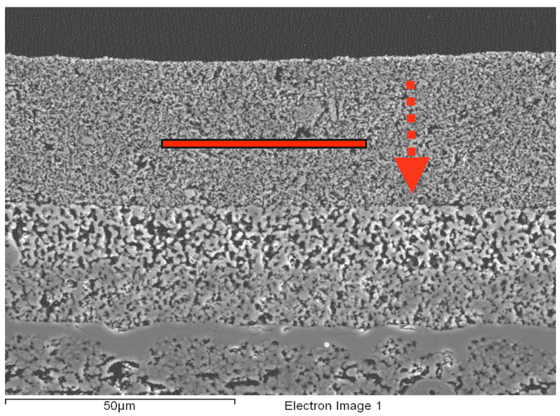

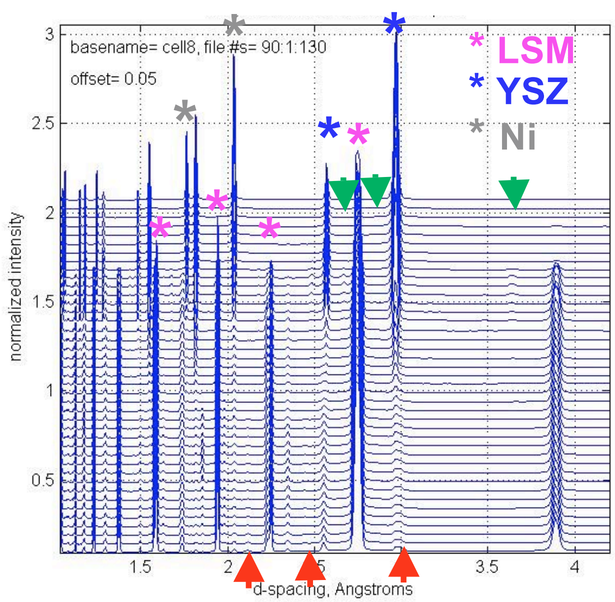

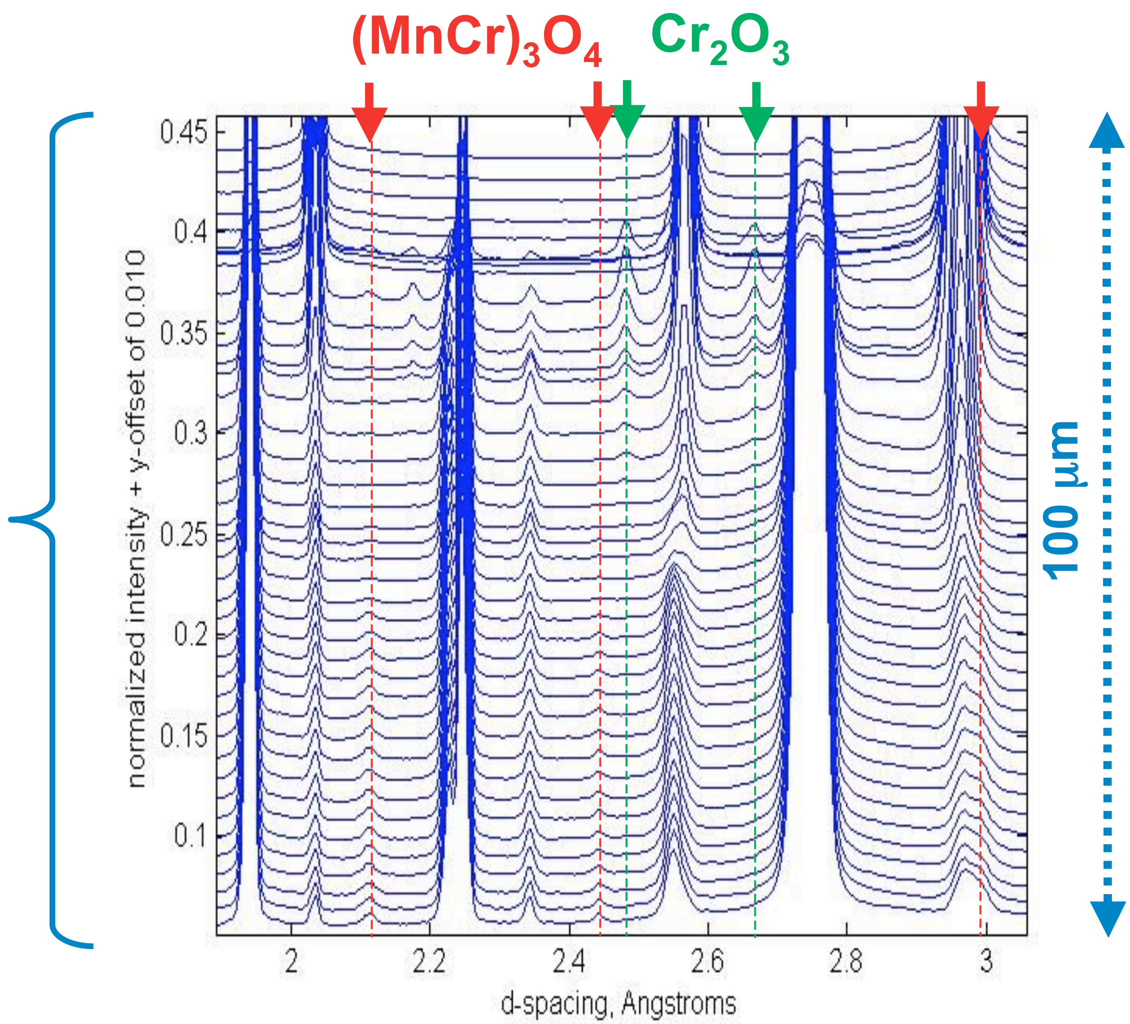

Vertical Scan thru Cathode Depth

GSAS refinement – interface region (5 phases)

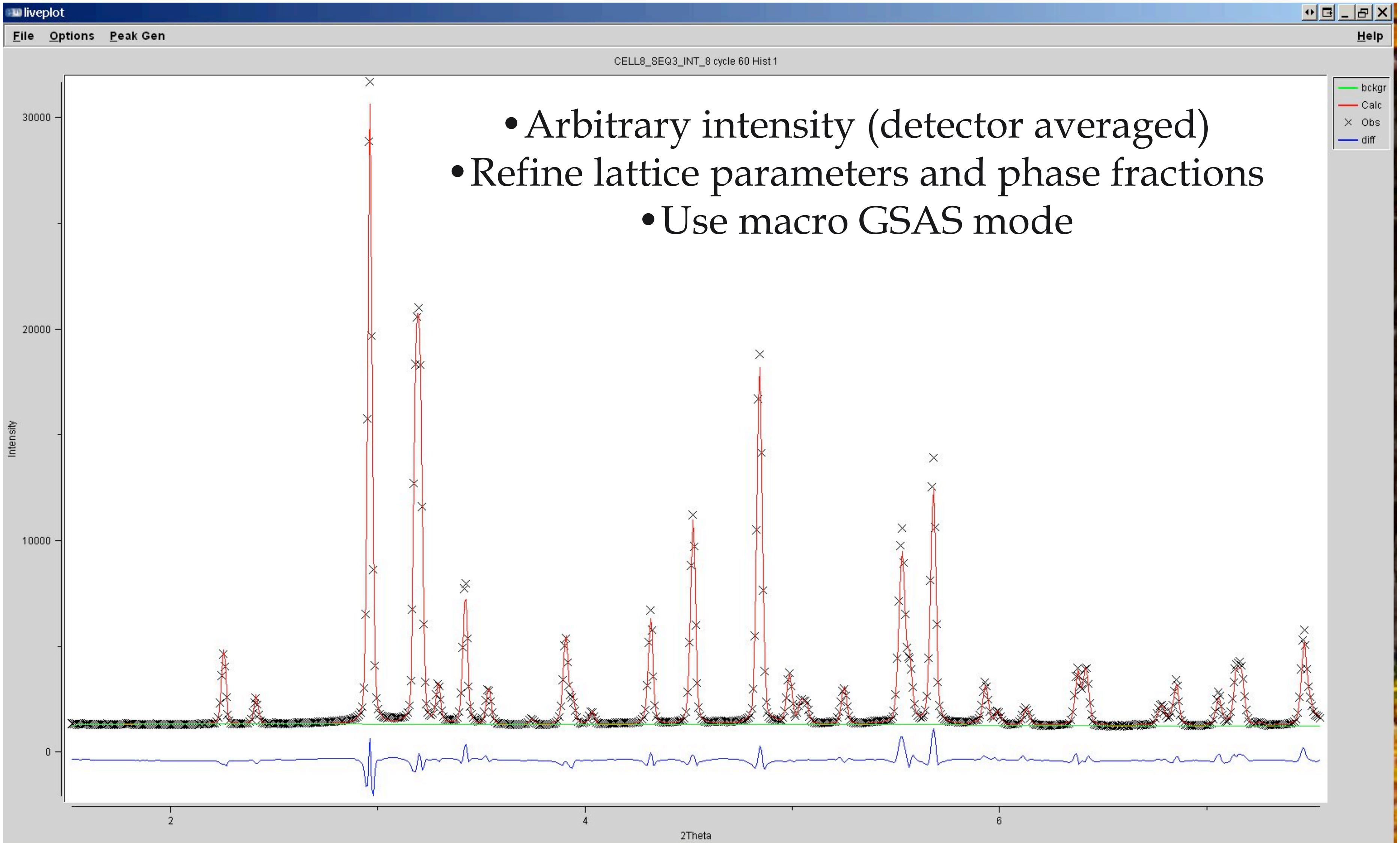

How $_{low}$ can you go?

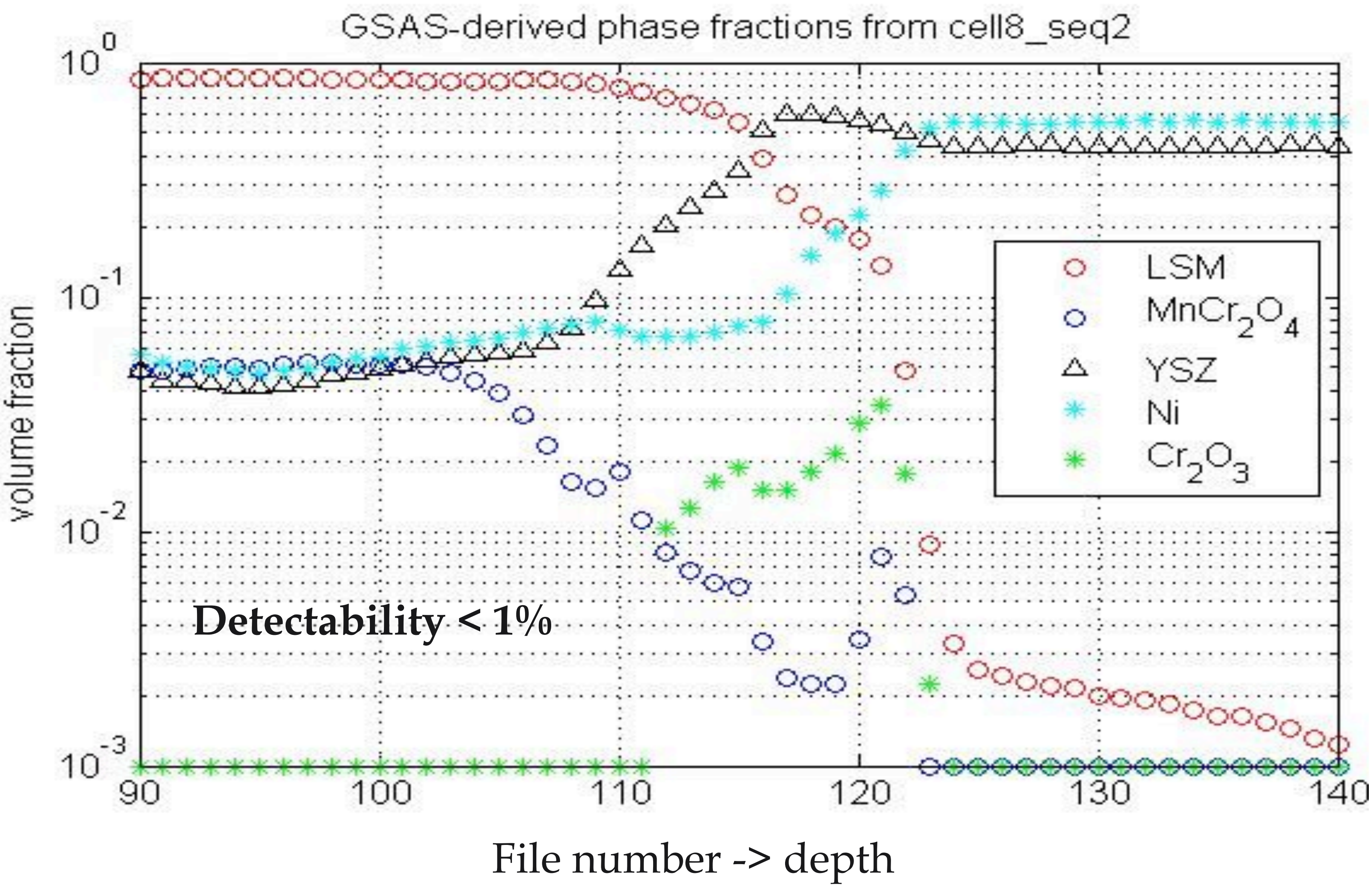

GSAS-derived weight fractions for 4/5 SOFC phases

- **Transition between 2 Cr phases in "active cathode" region**
- **Cr_2O_3 strongly associated with YSZ content and current collector position**
  - **suggests formation through electrochemical reduction**
- **Cr/Mn spinel has weaker spatial association**
  - **possibly formed by direct chemical process (Cr transport through gas & solid diffusion)**
- **A continuous layer of Cr_2O_3 built at the cathode/ electrolyte interface**
  - **probably plays a key role in raising impedance and blocking mass transfer**

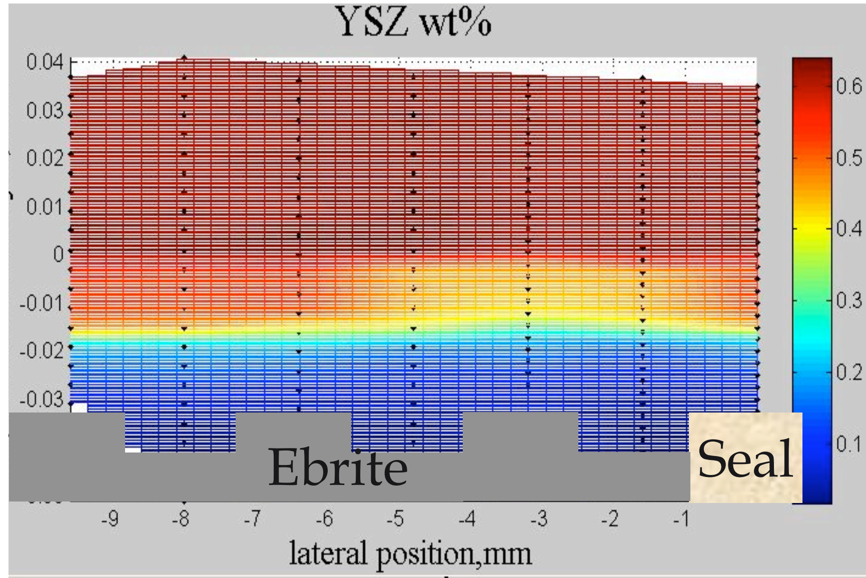

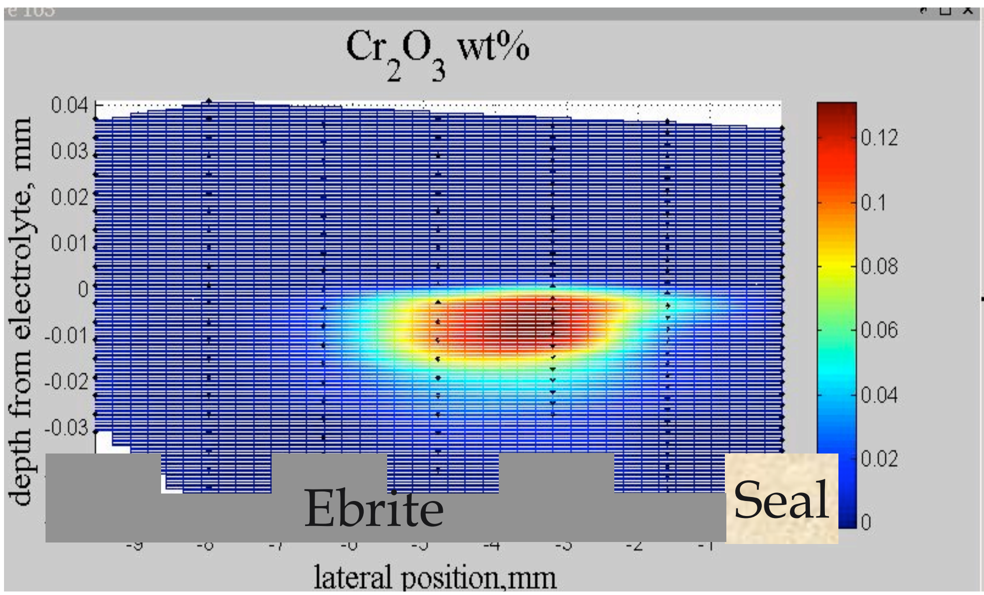

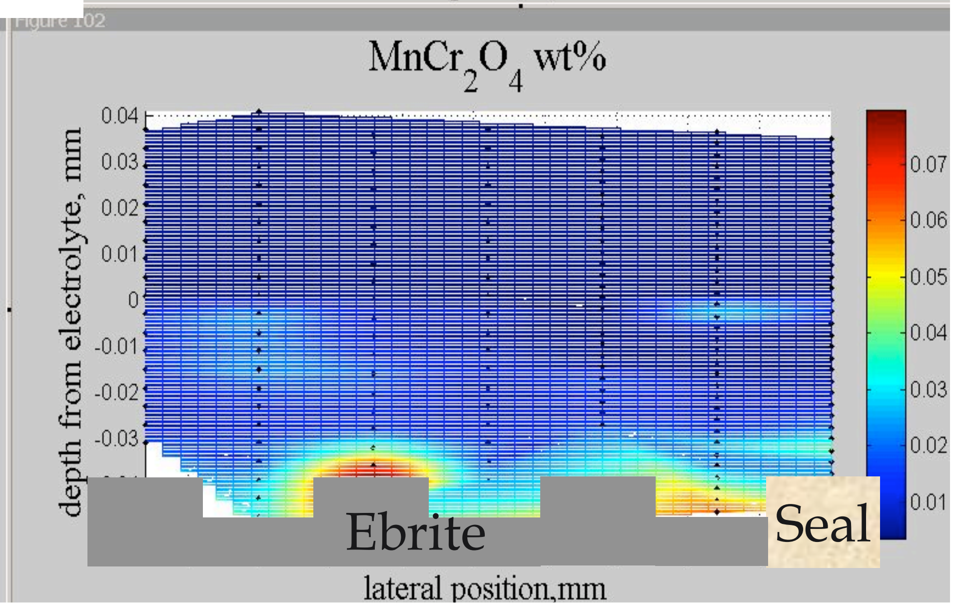

Cr_2O_3 and $(MnCr)_3O_4$ Phase and Concentration Distribution in Deactivated SOFC Cell

Cr Accumulation Mechanism

- Generation at metallic interconnect

$Cr_2O_3(s) + 1.5O_2(g) + 2H_2O(g) = 2CrO_2(OH)_2(g)$

- Deposition through Electrochemical Process

$2CrO_2(OH)_2(g) + 6\ e^- = Cr_2O_3(s) + 2H_2O(g) + 3O^{2-}$

- Deposition through Chemical Process

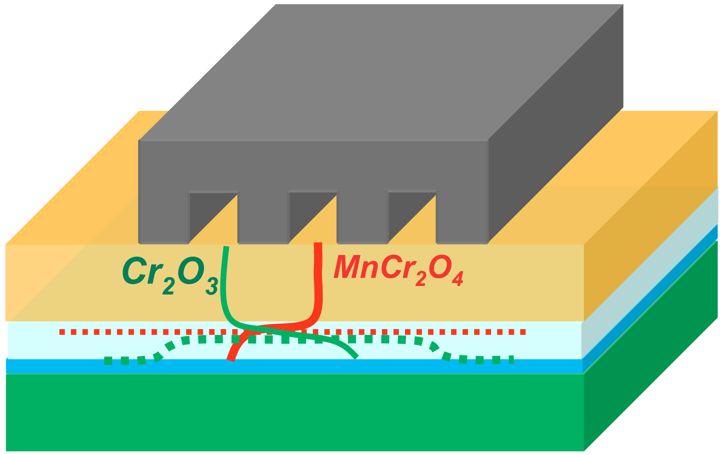

$3CrO_2(OH)_2(g) + La_{1-x}Sr_xMnO_3(s) = La_{1-x}Sr_xCrO_3(s) + MnCr_2O_4(s) + 3H_2O(g) + 2.5O_2$

K. Hilpert, D. Das, M. Miller, D. H. Peck and R. Weiß, *J. Electrochem. Soc.* **143**, 3642, 1996
S. P. S. Badwal, R. Deller, K. Foger, Y. Ramprakash, J. P. Zhang, *Solid State Ionics*, **99**, 297, 1997

Internal strain and intraphase composition versus depth

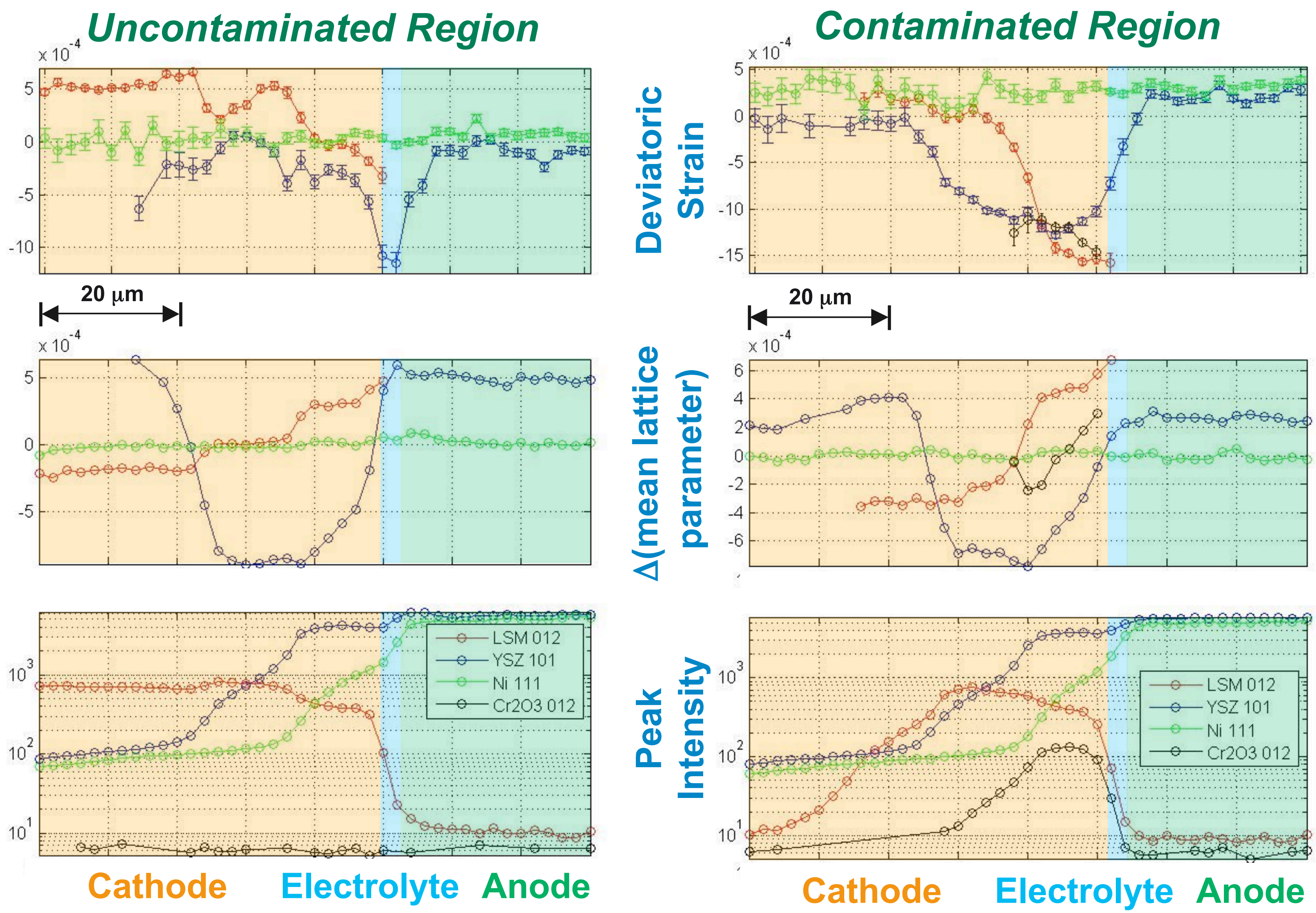

Case study II: Strain and stress mapping in advanced structural steels

Collaborators:

Yana Qian and Greg Olson

Northwestern University

Advanced structural steel

Material - *Ferrium®* C67

- Belongs to a new class of carburized secondary hardening gear and bearing steels, utilizing an efficient M2C precipitate strengthening dispersion.
- Combines a tough ductile core with an ultra-hard carburized case that can achieve hardness levels of up to 67 HRC, promoting high wear and contact fatigue life.
- Is the product of an ongoing research and development program with the objective of reducing gear weight by as much as 50% over conventional carburized gear steels.

US Patent Number 6,176,946 B1

Application

- High power density transmission systems: helicopters, heavy machinery, racing, and manufacturing.

Material Properties

Temper	YS (ksi)	UTS (ksi)	El (%)	Core Hardness (HRC)	Case Hardness (HRC)
Overage	180	230	17	48-50	65-67

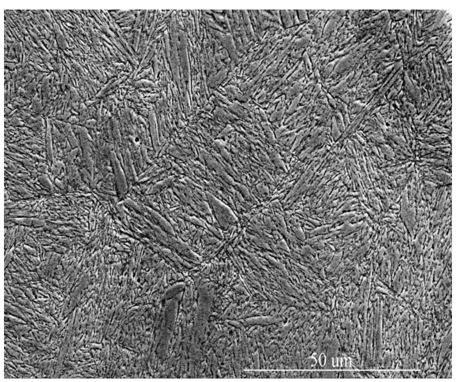

C67 microstructure (SEM)

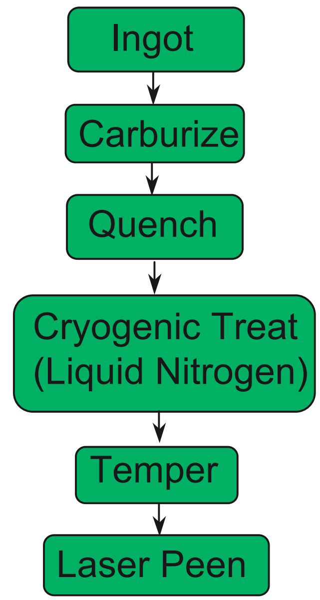

Material Processing

Laser Peening

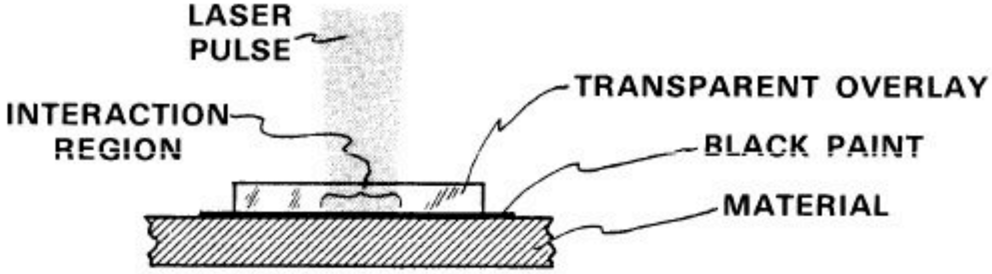

a. Surface area to be laser shocked, showing the laser beam and overlays.

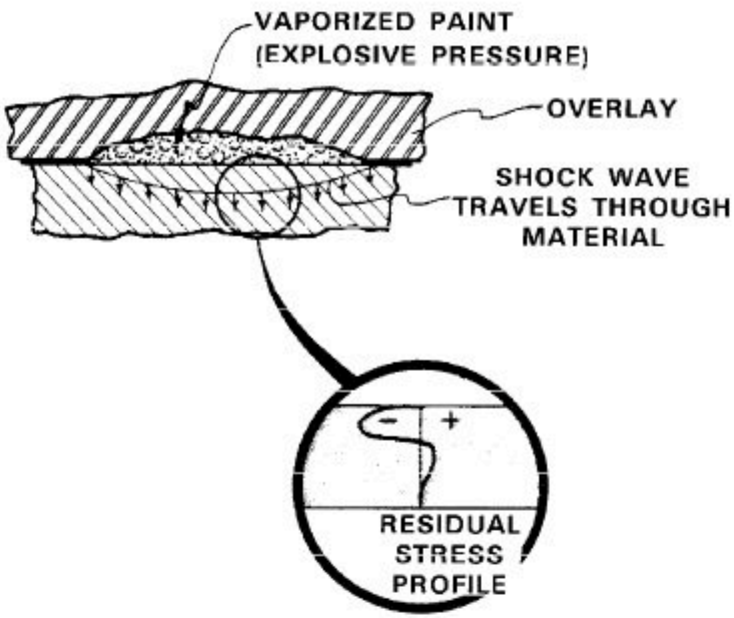

b. Effect of laser beam at the overlay-workpiece interface.

Ref: Laser Shock Processing Technical Bulletin No. 1, LSP Technologies, Inc.

Experimental geometry for non-destructive mapping

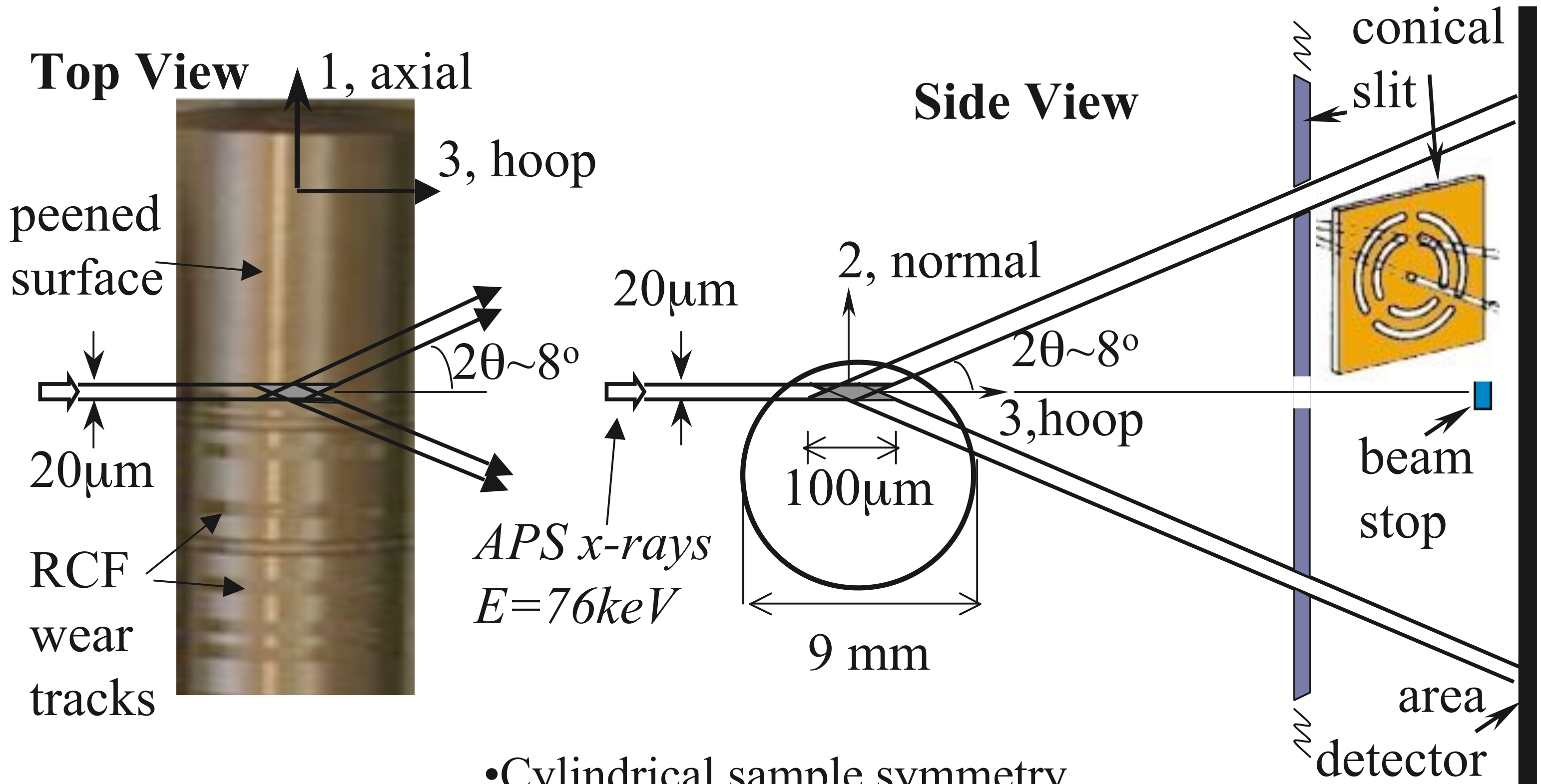

- Cylindrical sample symmetry
  - rotate for grain averaging
- Conical slit
  - 3-d gage volume (~20x20x150 um^3)
  - normal & axial components simultaneously
- move sample in x2 for depth resolution

Wear samples
- Ground
- Shot peened
- Laser peened

Diffraction Patterns from sample

Without Conical Slit

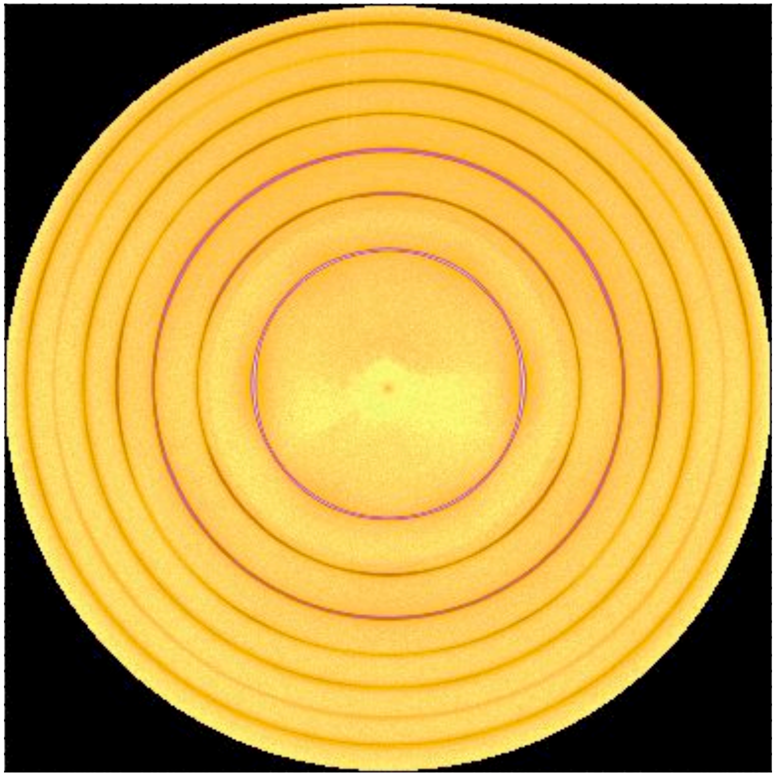

Powder Diffraction

7 BCC reflections

With Conical Slit

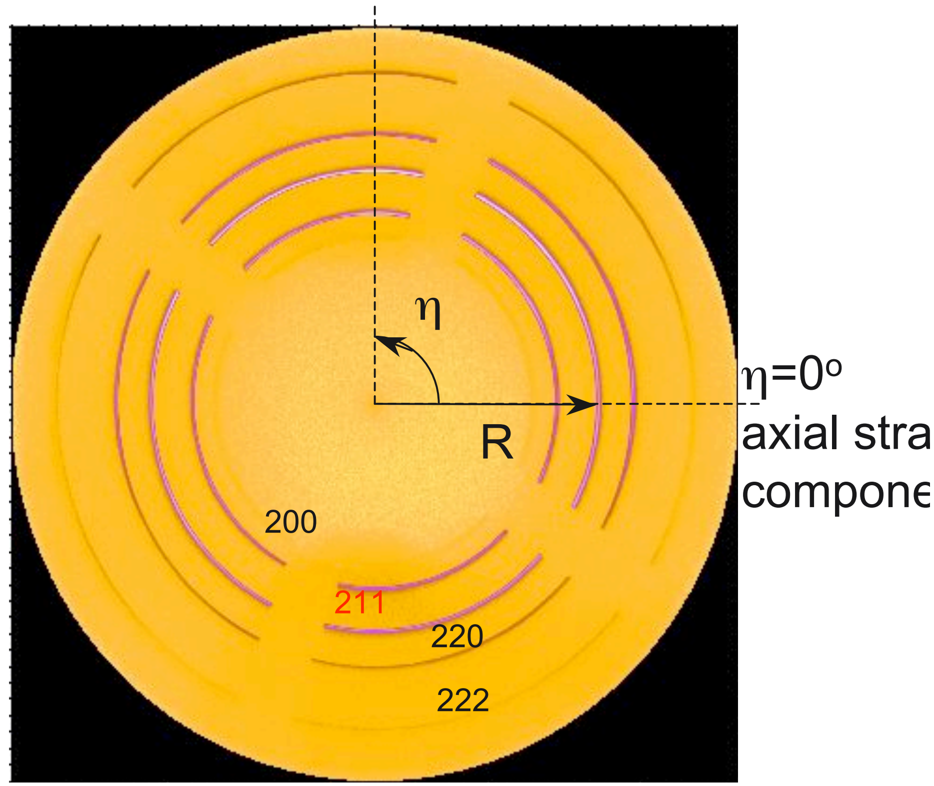

4 BCC Reflections

(211) is chosen for analysis.

Peak position versus orientation – deviatoric strain

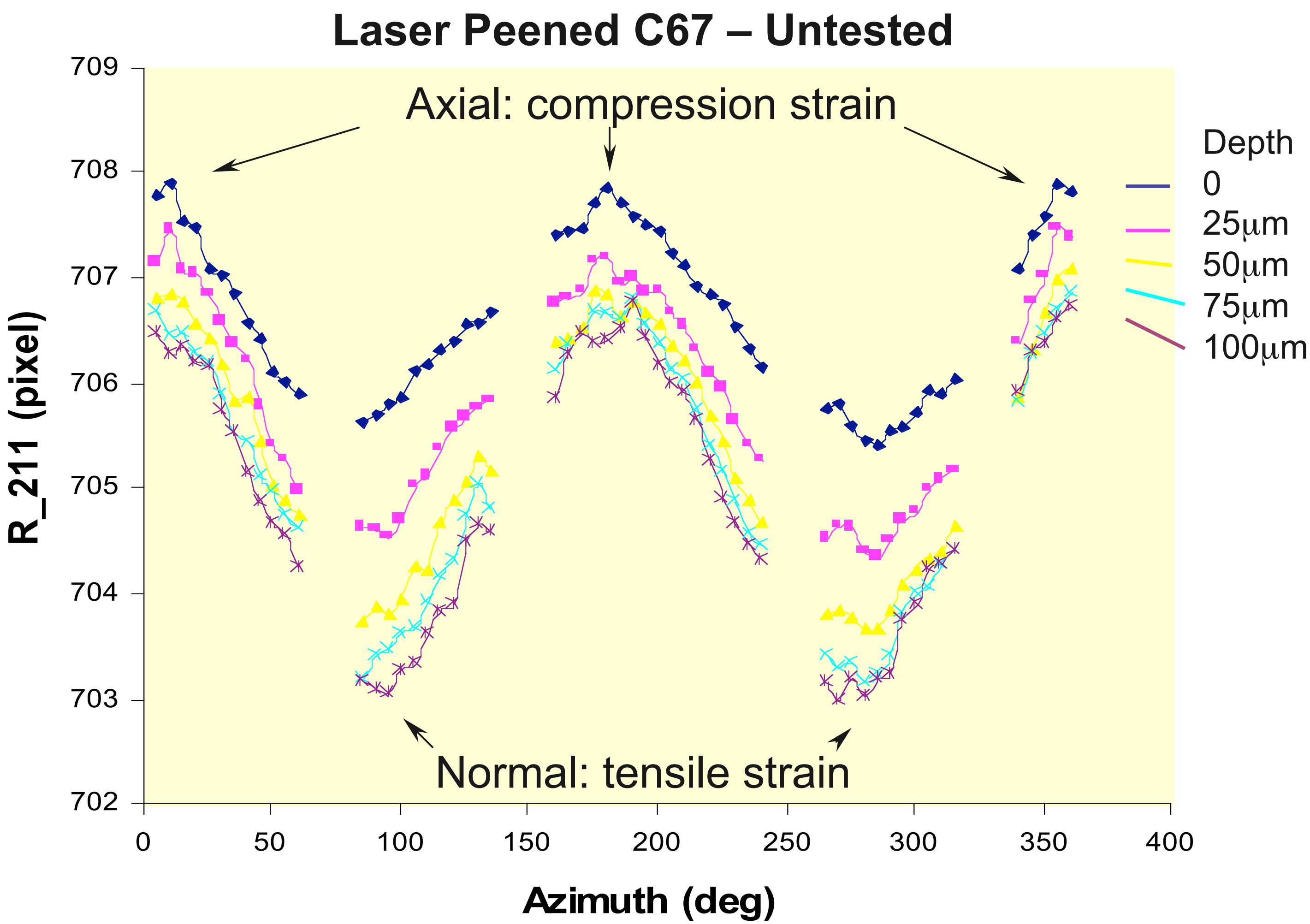

Residual Strain vs Depth – 3 conditions

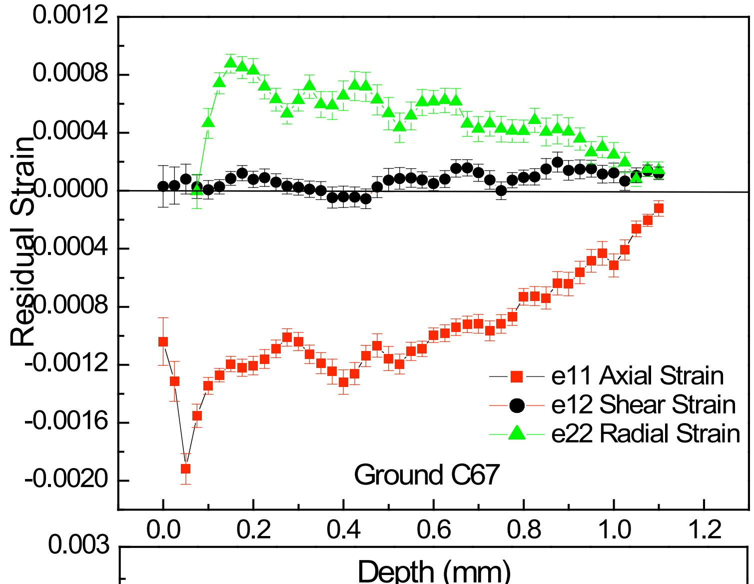

- Results for martensite (211):
- 3 measured strain components
- regions away from wear tracks
- 25 um step width

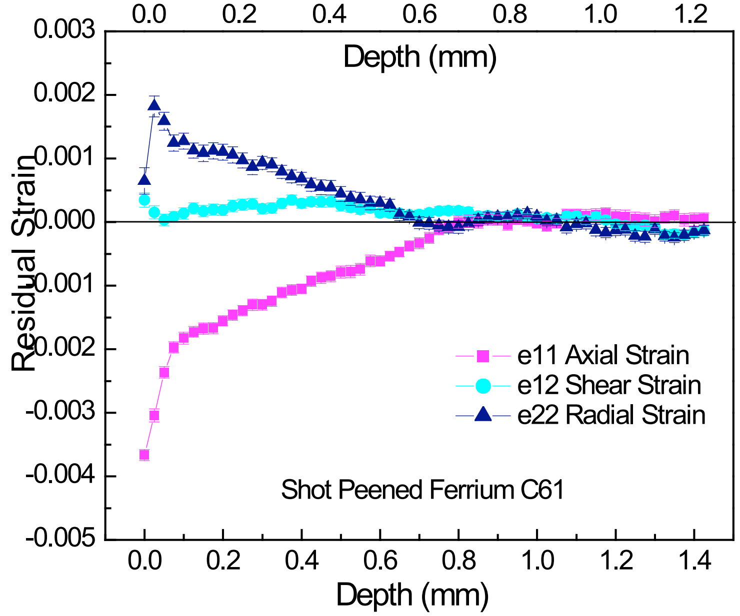

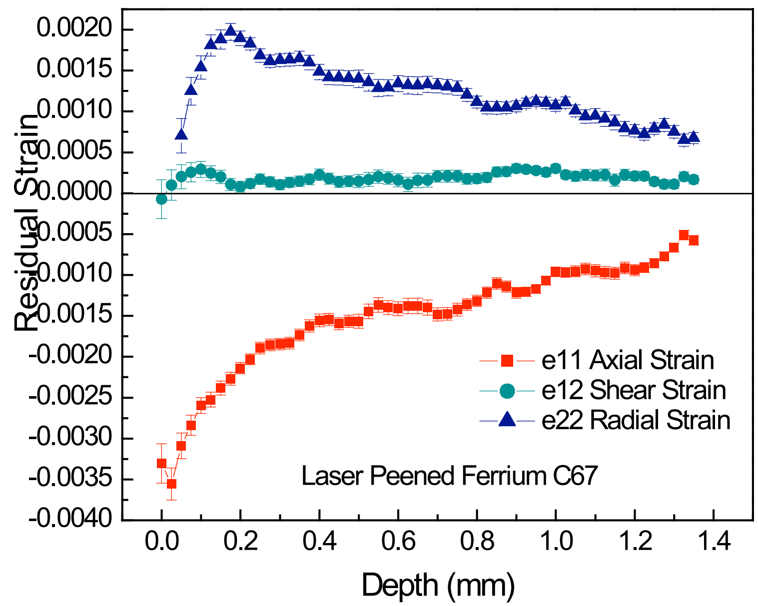

Residual Stress vs Depth, Laser-Peened Sample

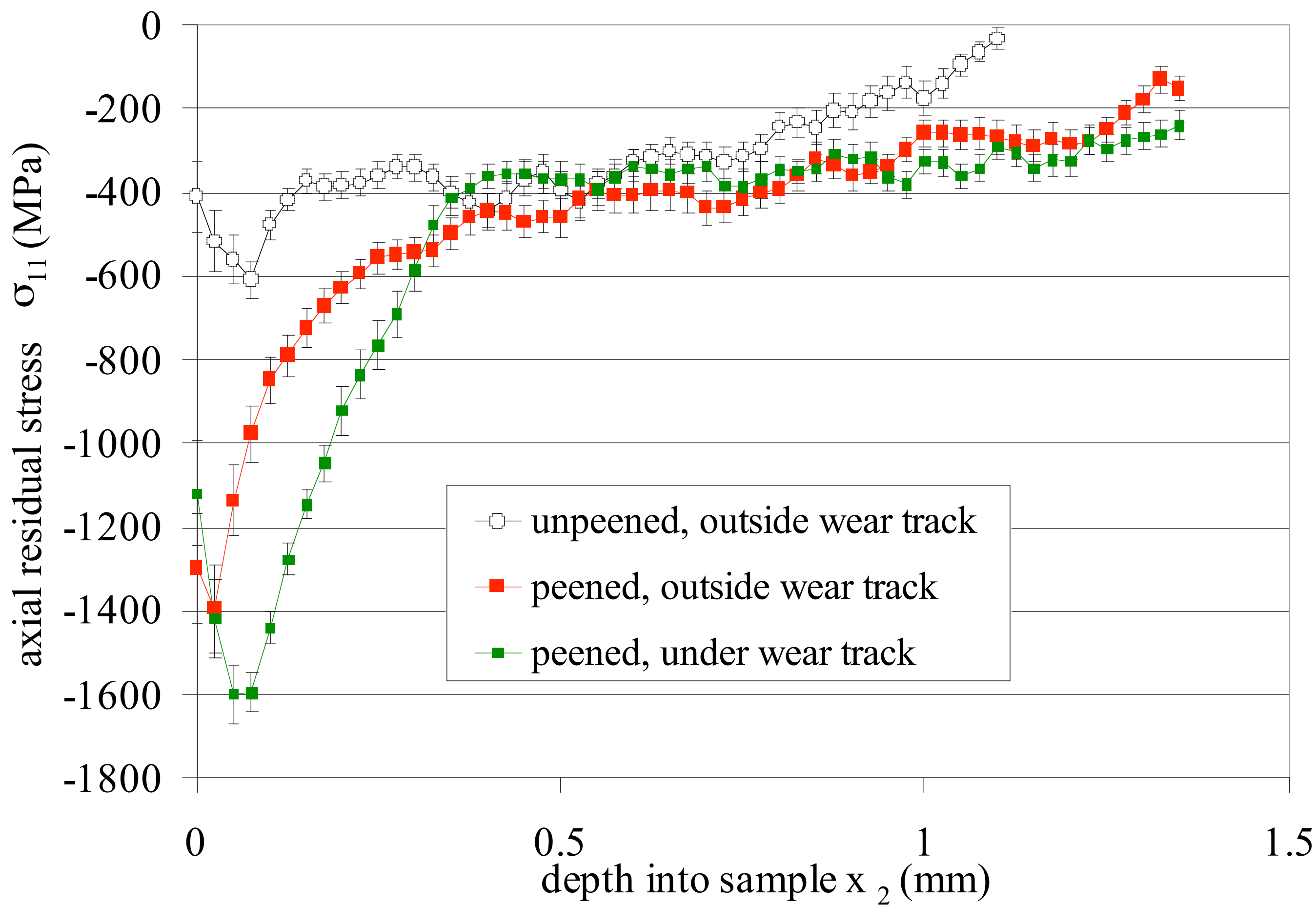

Main observations

- Significant compressive residual stresses due to initial thermo-mechanical processing
- Increase in RS after laser peening
- After RCF, RS maximum shifts to subsurface, no appreciable fading

Additional microstructural information: peak broadening vs depth

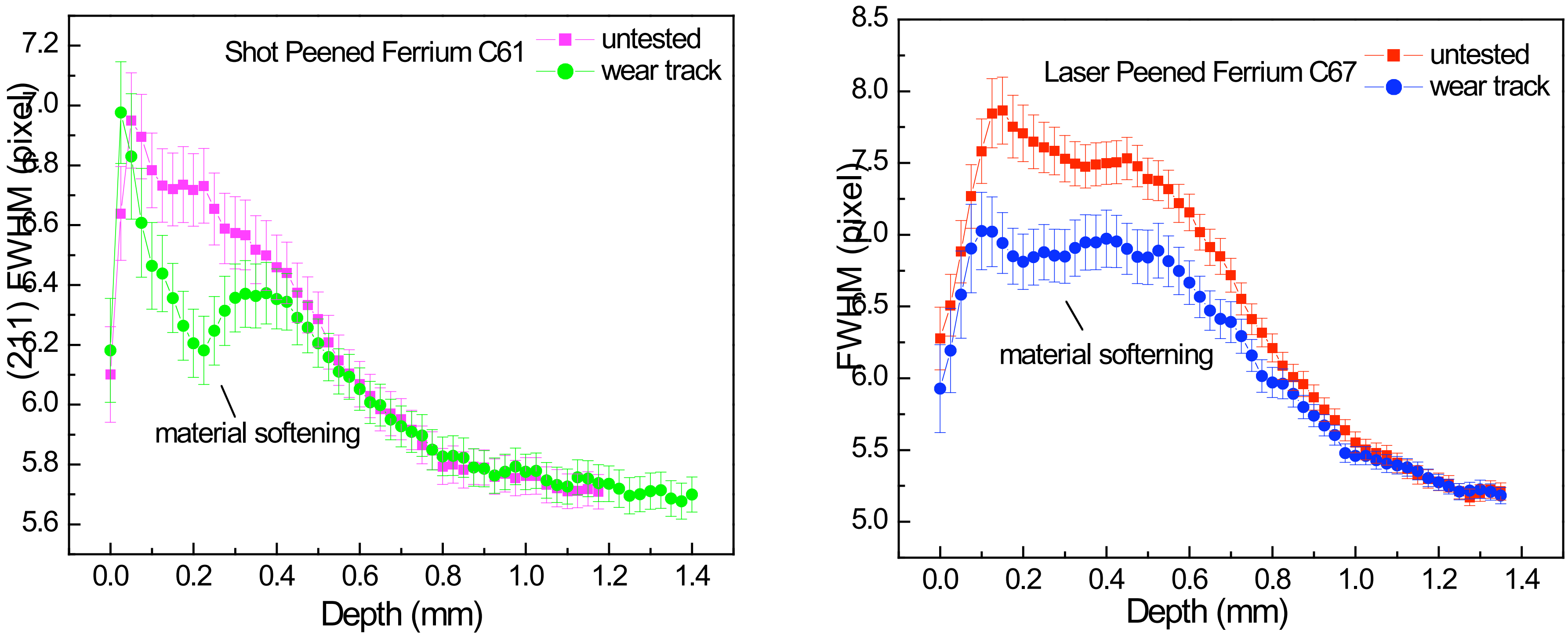

RCF wear induces reduction in peak broadening

– lower martensite fraction and/or defect density

Confirmation of microstructural changes with optical microscopy

Laser Peened C67 Cross Section Optical Images

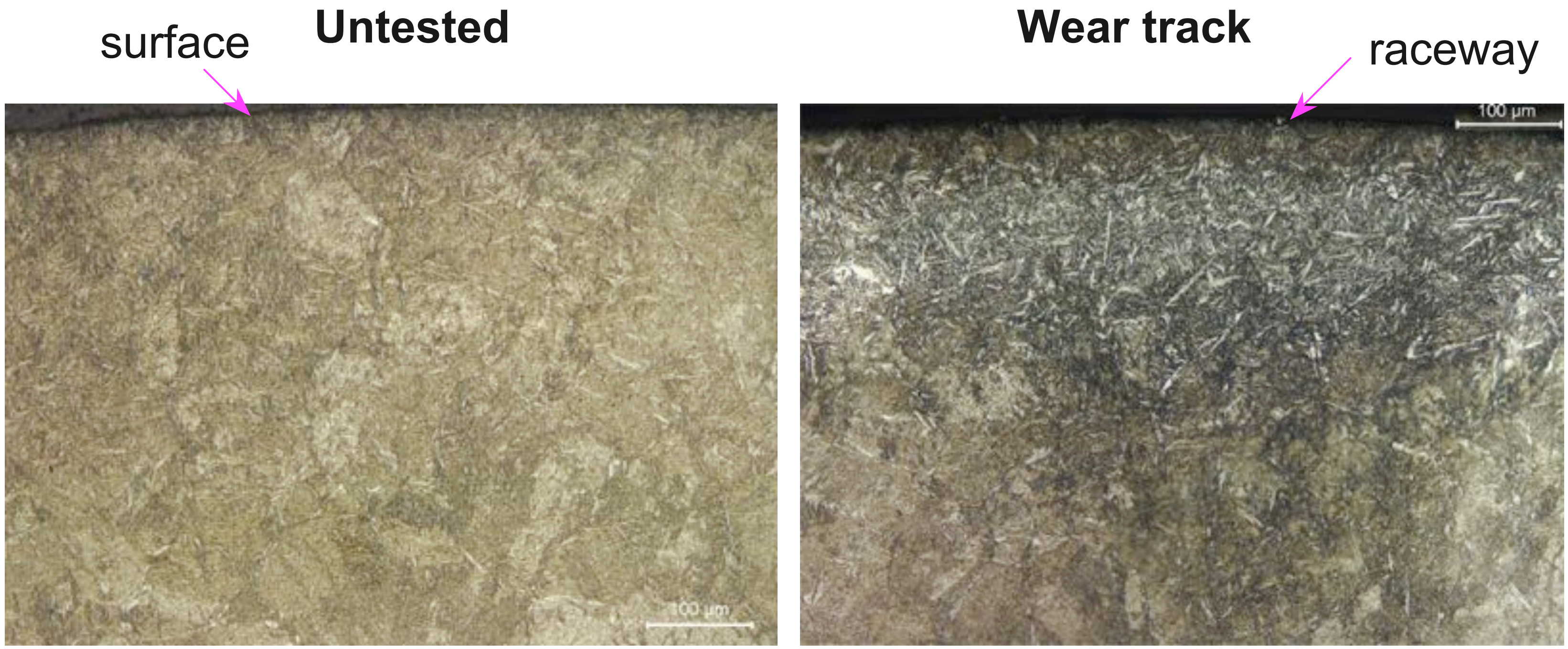

Microstructure alters during rolling contact fatigue, suggesting partial transformation from martensite to ferrite.

Summary and Outlook

- High-energy x-ray scattering is a powerful technique for materials investigation
- Sector 1 instrument benefits from:
  - 7 GeV synchrotron + undulator source
  - Optics:
    - *Brilliance-preserving monochromator*
    - *Refractive focusing lenses*
    - *Conical slit*
  - Two-dimensional detectors (fast and large)
- Solid –oxide fuel cell stack
  - Gage volume ~2x50x1000 um^3
  - Phase ID – yields information on mechanism of Cr-poisoning
  - Strain – TEC differences are non-negligible, Cr_2O_3 induces additional strain.
  - Lattice parameter – stoichiometry variations clearly seen
  - Future *in situ* studies are envisioned
- Advanced structural steel
  - 3-d gage volume~20x20x150 um^3
  - High residual stresses due to laser and shot-peening
  - Stress relaxation under wear tracks

Potential New Applications of Microfocused X-ray Scattering Technique for the Study of SOFCs

- New phase identification at different boundary and depth of layers
- Solid state interfacial reaction between different phases
- 3-D strain and lattice deficiency distribution
- Density, surface area, porosity, grain size and morphology changes in SOFC at micron spatial resolution
- *In-situ,* real-time study at elevated temperature (1000 °C, 50~100 °C/sec)
- *In-situ,* real-time study under SOFC operating conditions

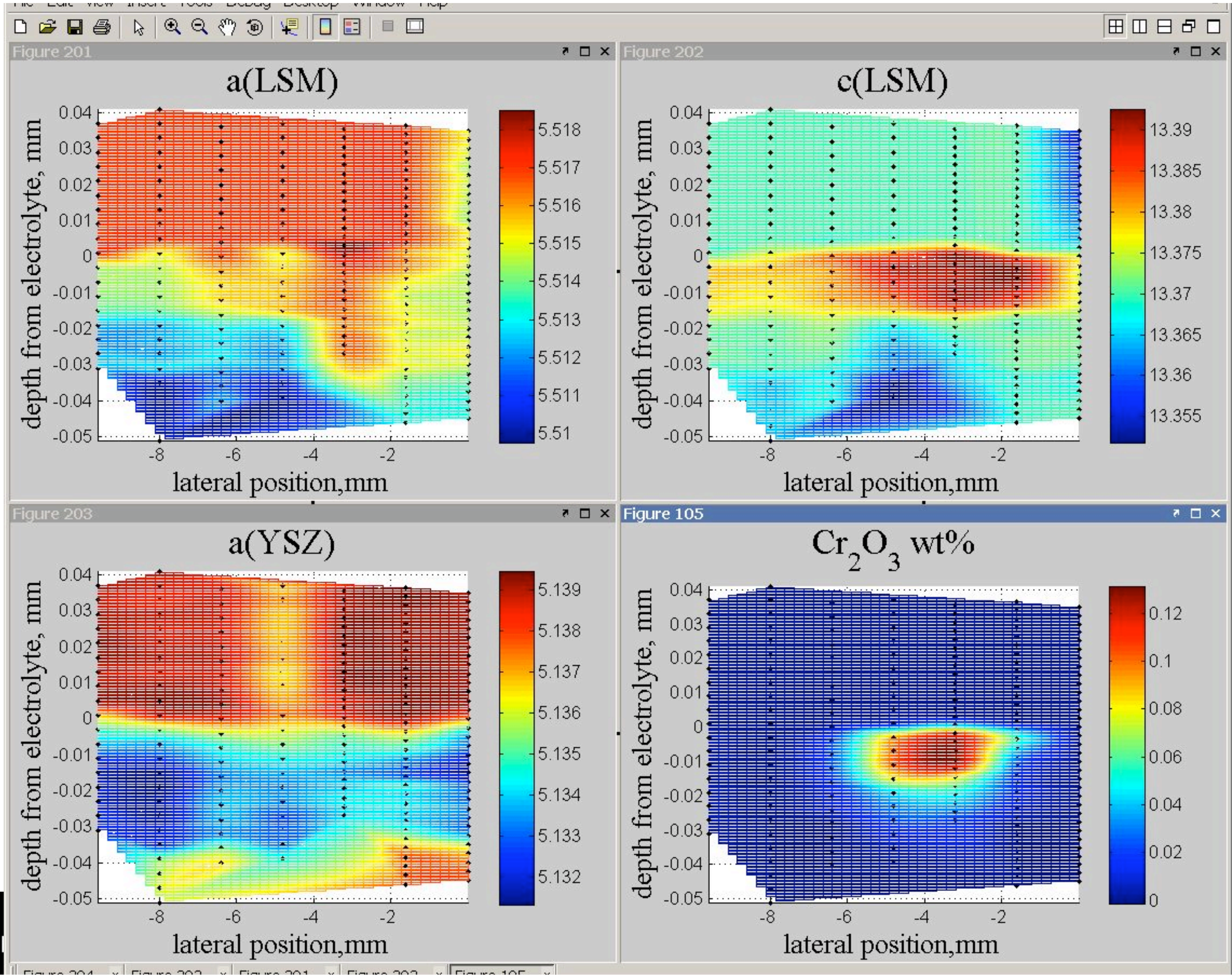
Figure 201
a(LSM)
depth from electrolyte, mm
lateral position,mm
5.518
5.517
5.516
5.515
5.514
5.513
5.512
5.511
5.51
Figure 202
c(LSM)
depth from electrolyte, mm
lateral position,mm
13.39
13.385
13.38
13.375
13.37
13.365
13.36
13.355
Figure 203
a(YSZ)
depth from electrolyte, mm
lateral position,mm
5.139
5.138
5.137
5.136
5.135
5.134
5.133
5.132
Figure 105
Cr2O3 wt%
depth from electrolyte, mm
lateral position,mm
0.12
0.1
0.08
0.06
0.04
0.02
0
0.04
0.03
0.02
0.01
0
-0.01
-0.02
-0.03
-0.04
-0.05
-8
-6
-4
-2

Accumulation of Cr_2O_3 Induces Deviatoric Strains on All Phases

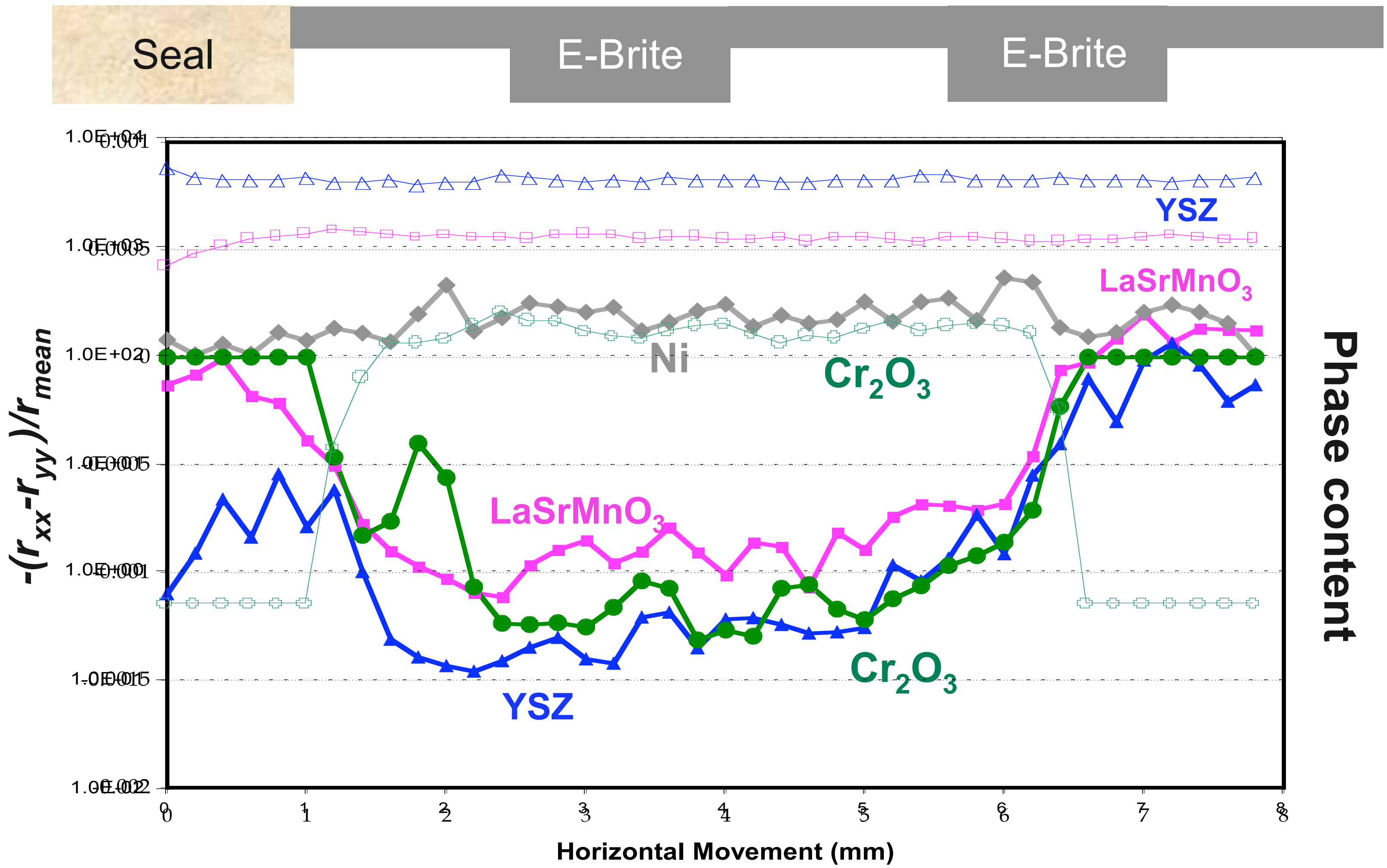

In-plane compressive strains are directly associated with Cr_2O_3 buildup

Distribution of Different Cr Phases as a Function of Cathode Depth